

## Mechanistic insights into the phenomena of increasing capacity with cycle number: Using pulsed-laser deposited MoO<sub>2</sub> thin film electrodes

Michael Fenech<sup>a</sup>, Sean Lim<sup>b</sup>, Jeffrey Cheung<sup>c</sup>, Neeraj Sharma<sup>a,\*</sup>

<sup>a</sup> School of Chemistry, UNSW Sydney, NSW 2052, Australia

<sup>b</sup> Electron Microscope Unit, Mark Wainwright Analytical Centre, UNSW Sydney, NSW 2052, Australia

<sup>c</sup> Australian National Fabrication Facility, UNSW Sydney, NSW 2052, Australia.

### Supporting information

The air sensitivity of the films and oxidation state mix were determined using XPS and compared to the literature (55), Figure 1b and 1c, Table S1. The XPS data contains the characteristic three peak shapes consistent with MoO<sub>2</sub> (55,56). The levels of Mo<sup>δ+</sup> ( $\delta: 0 < \delta < 4$ ) and Mo<sup>4+</sup> remain unchanged in both films. However, in a film that was specifically exposed to air the Mo<sup>5+</sup> oxidation state decreases from 18% to 14% and the Mo<sup>6+</sup> oxidation state increases from 16% to 20%. This indicates slight surface oxidation does occur in air.

Table (S1) XPS binding energies and oxidation states, bottom two rows are this work.

	Mo3d <sub>3/2</sub>				Mo3d <sub>5/2</sub>			
	Mo <sup>δ+</sup>	Mo <sup>4+</sup>	Mo <sup>5+</sup>	Mo <sup>6+</sup>	Mo <sup>δ+</sup>	Mo <sup>4+</sup>	Mo <sup>5+</sup>	Mo <sup>6+</sup>
<b>MoO<sub>2</sub></b>	-	233.1(13)	-	235.4(29)	-	230.0(16)	-	232.3(42)
<b>MoO<sub>2</sub>-r1</b>	231.8(5)	233.2(18)	234.3(8)	235.7(7)	228.7(7)	230.1(31)	231.2(13)	232.6(11)
<b>MoO<sub>2</sub>-r3</b>	231.8(17)	233.1(9)	234.0(12)	235.6(3)	228.7(25)	230.0(13)	230.9(16)	232.5(5)
<b>MoO<sub>2</sub>-Air</b>	233.0(12)	233.6(4)	234.3(14)	236.2(20)	229.7(12)	230.2(4)	230.9(14)	232.9(20)
<b>MoO<sub>2</sub>-Ar</b>	232.8(12)	233.4(4)	234.0(18)	235.9(16)	229.6(12)	230.1(4)	230.6(18)	232.6(16)

( ): area percent

r1,r3: reduced in H<sub>2</sub> at 673 K for 1 and 3 h, respectively (55)

δ: 0 < δ < 4 in oxidation state

In order to determine the thickness of the film which is critical for mass calculations and determining capacity, representative films were milled (FIB) and cross sectional SEM images taken as shown in Figure S1. Figure S1 shows a film deposited at 1.5 J/cm<sup>2</sup> at 300 °C in a chamber pressure of 10<sup>-6</sup> Torr with thickness of 103.1 ± 7.9 nm on a thin Cu substrate.

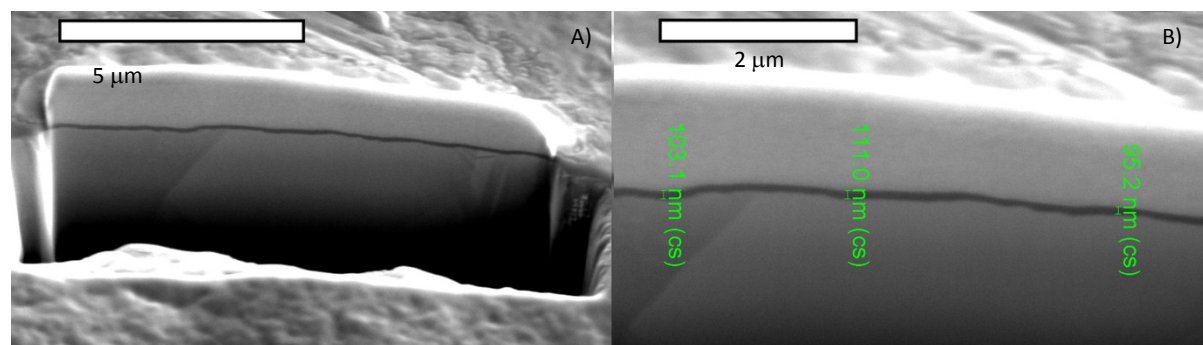


Figure S1(a). A cross sectional SEM image of a MoO<sub>2</sub> film with a platinum deposit to protect the surface before it is milled out with a FIB, and (b) the same film at higher magnification with thickness measurements.

TEM analysis was undertaken on certain films to obtain higher resolution images of thicknesses and the films themselves. Figure S2 shows a film that was deposited at 8.7 J/cm<sup>2</sup> at 300 °C in chamber pressure of 10<sup>-8</sup> Torr with a thickness of 420 ± 18 nm on a thick Cu substrate. Both SEM and TEM images illustrate a significant variation in film thickness on the order of 3-4%. EDS data shows the elemental distribution of the film with the Mo-rich thin film layer clearly highlighted.

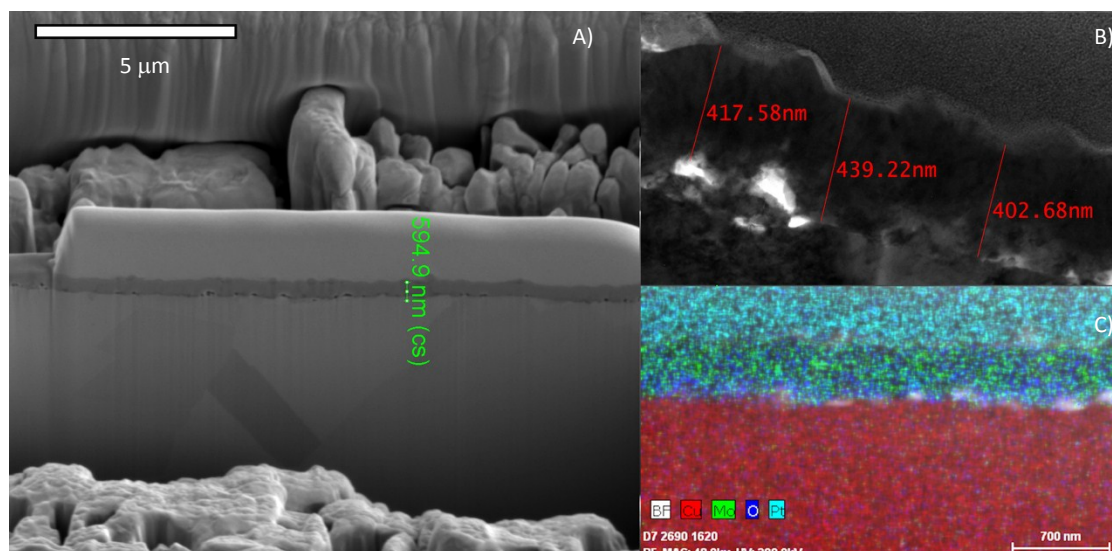


Figure S2(a). SEM cross section image demonstrating the section that was milled by FIB. (b) The same cross section of MoO<sub>2</sub> film on thick Cu substrate containing thickness measurements via TEM and (c) TEM EDX map showing elemental composition of a cross section of MoO<sub>2</sub> film.

### Temperature growth space

Variation of substrate temperature was explored and the results are presented in Table S1. All parameters were kept the same except temperature and small changes in laser intensity which could not be avoided. As temperature increases an increased ordering of the material was observed as more particles appear on the surface of films, with 300 and 450°C growth resulting in fused particles that still feature rectangular rod like structures (see Figure S3). FIB-SEM cross sectional images appear to show no linear trend in regard to thickness and temperature (Table S1). The film deposited at 150°C is much less uniform in thickness while the film deposited at 450°C is much thinner and has no pores visible between the substrate and the film (see Figure S4). The variation in thickness and no clear trend indicates the importance of using measurement techniques like SEM or TEM to determine thickness in order to ascertain reliable capacity values with appropriate errors. The images clearly show that the variation is significant and that researchers need to take this into account for final reporting. It is interesting to note the wave like modulation in certain samples with uplifted areas which speculatively can be locations where delamination or failure of the films with cycling could occur.

There seems to be a trend with increasing substrate temperatures of increasing the maximum capacities observed and the number of cycles before the peak capacity or maxima in capacity is achieved (see arrows in Figure S4). Transition metal oxides show evidence of capacities increasing with cycling, (57-62) there is nothing reported of the magnitude observed here in the literature to date. The films grown at 150 and 300°C also show early signs of the capacity increasing again with further cycling. The film deposited at 300°C has the most interesting features, including densely packed uniform surface topography and relatively high maximum capacity compared to its initial capacity.

Table (S2) Summary of the thin film growth conditions, structural and electrochemical characterisation for films grown at different substrate temperatures.

Substrate Temp (°C)	Laser fluence (J/cm <sup>2</sup> )	Film thickness (nm)	Film mass (mg)	Initial capacity (mAh/g)	1st peak	
					mAh/g	Cycle #
RT	2.9	239 ± 20	0.15 ± 0.01	471 ± 61	-	-
150	2.8	273 ± 146	0.18 ± 0.06	636 ± 482	567 ± 430	50
300	2.4	232 ± 46	0.15 ± 0.01	420 ± 58	666 ± 462	62
450	2.7	102 ± 21	0.07 ± 0.05	867 ± 555	790 ± 110	91

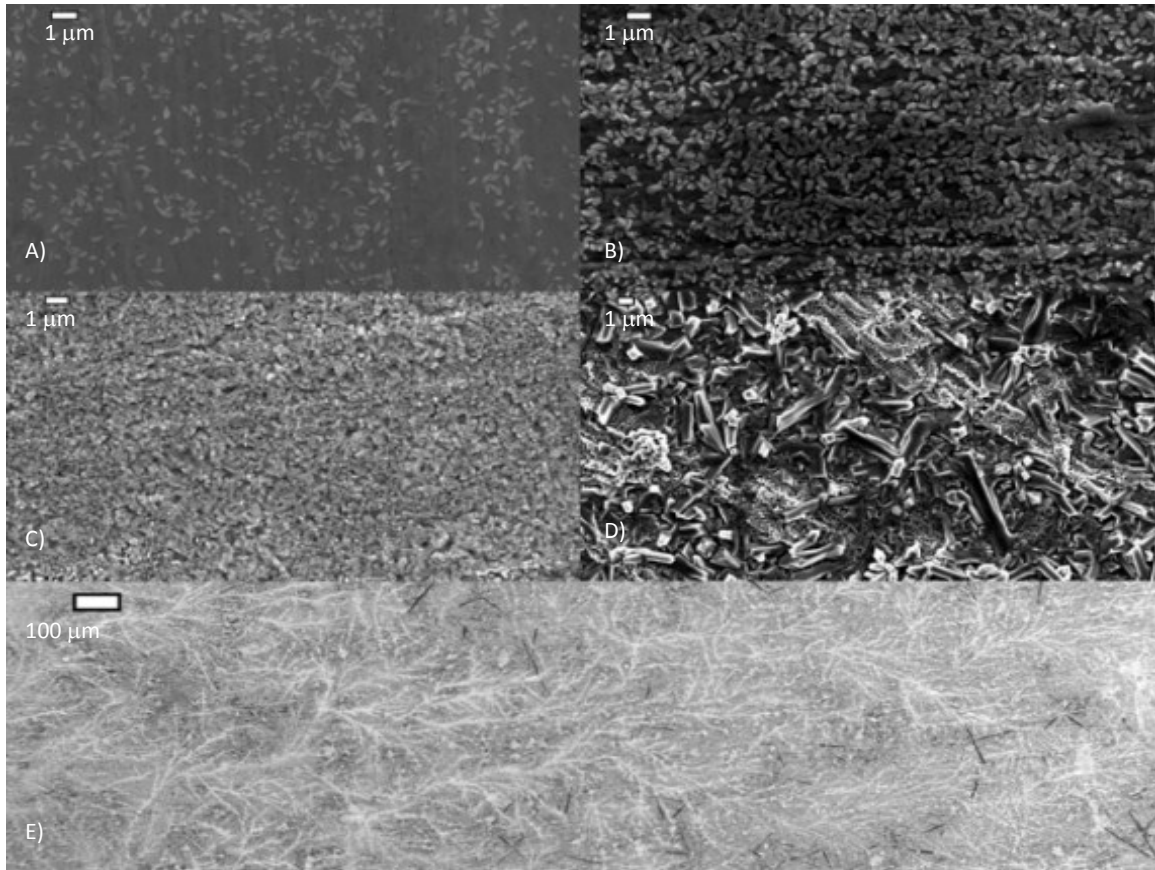


Figure S3. SEM images of MoO<sub>3</sub> films grown at (a) RT, (b) 150°C, (c) 300°C and (d) 450°C. All images are taken at the same magnification with the exception of (e) MoO<sub>3</sub> film grown at 450°C with lower magnification.

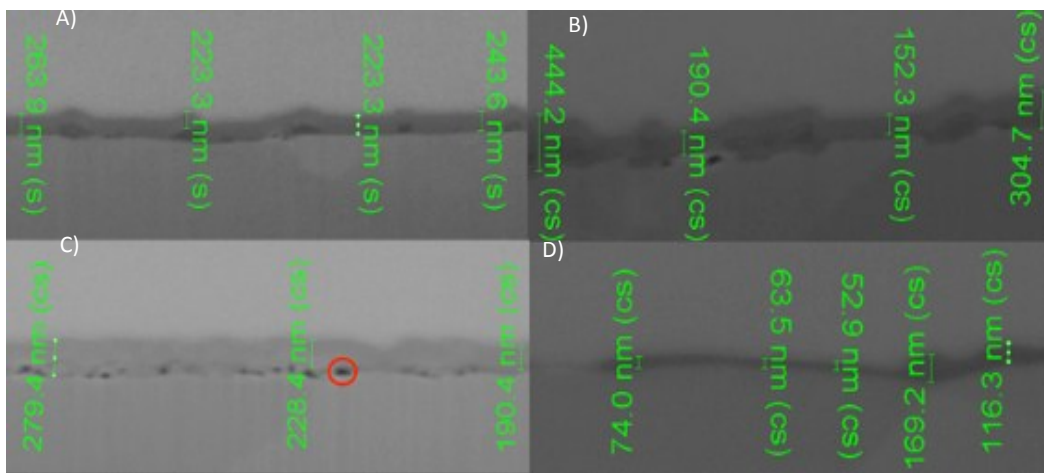
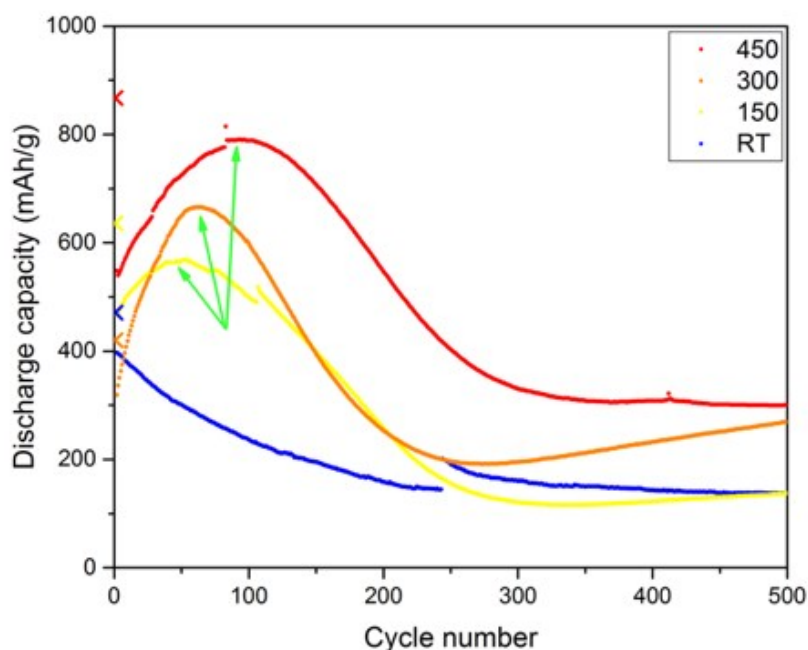


Figure S4. FIB cross sectional images with films deposited with substrate temperatures of (a) RT, (b) 150°C, (c) 300°C and (d) 450°C. The red circle indicates a pore between the substrate and the film.

Figure S5. Cycling performance of films deposited with different substrate temperatures. The plot shows the discharge capacity as a function of cycle number. The X for each temperature represents the initial cycle. The arrows show the increasing capacity and cycle number for the peak capacity for films deposited with increasing temperatures. Temperature is indicated in the legend.



#### Laser fluence

Table S3 shows a summary of the effect of varying laser deposition energy has on the films structural characteristics and electrochemical performance. All films were deposited with a target rotation speed of 30 rpm for the duration of the deposition. Note, there is an unfortunate variation in current and this will be discussed below. The film deposited at 1.5 J/cm<sup>2</sup> has the highest applied current rate of 7.7 A/g during electrochemical characterisation. This film also has the highest observed capacity of 680 mAh/g. As higher current rates are generally associated with lower capacities this is an interesting result. It is expected that this result has more to do with the thickness, roughness and mass of the films. A factor that is worthy of consideration is the number of cycles before the peak capacity in the cycling data, which appears at 259, 119, 50 and 18 cycles for the 1.5, 1.6, 6.6 and 8.7 J/cm<sup>2</sup> films respectively. The general trend appears that the peak capacity occurs after a longer number of cycles for the lower energy laser pulses. Figure S6 shows the number of cycles it takes to reach the peak capacity with respect to laser energy.

Maintaining high laser fluence throughout a single deposition was made difficult by molybdenum oxide layers forming on the laser windows. This resulted in absorption losses at the laser window, reducing the overall fluence at the target as the deposition progresses. That is, with higher laser fluence, a larger plume is created which coats the laser window and therefore reduces the laser fluence target in subsequent pulses. Thus, higher laser fluence growth conditions typically have a reduction in laser fluence by the end of growth, with a film deposited at 8.74 J/cm<sup>2</sup> having a reduction of approximately 49% during its deposition.

Table (S3) Summary of the film growth conditions and associated electrochemical performance of films grown at different laser intensities.

Laser intensity (J/cm <sup>2</sup> )	Film thickness (nm)	Current rate (A/g)	Initial capacity (mAh/g)	Lowest capacity		Peak capacity	
				(mAh/g)	Cycle #	(mAh/g)	Cycle #
1.5	101 ± 4	7.7 ± 0.6	281 ± 22	272 ± 21	10	680 ± 53	259
1.6	108 ± 4	7 ± 0.6	228 ± 18	154 ± 12	2	472 ± 37	119
6.6	394 ± 15	2 ± 0.2	720 ± 56	515 ± 40	2	656 ± 51	50
8.7	417 ± 16	1.7 ± 0.1	640 ± 50	545 ± 43	3	614 ± 48	18

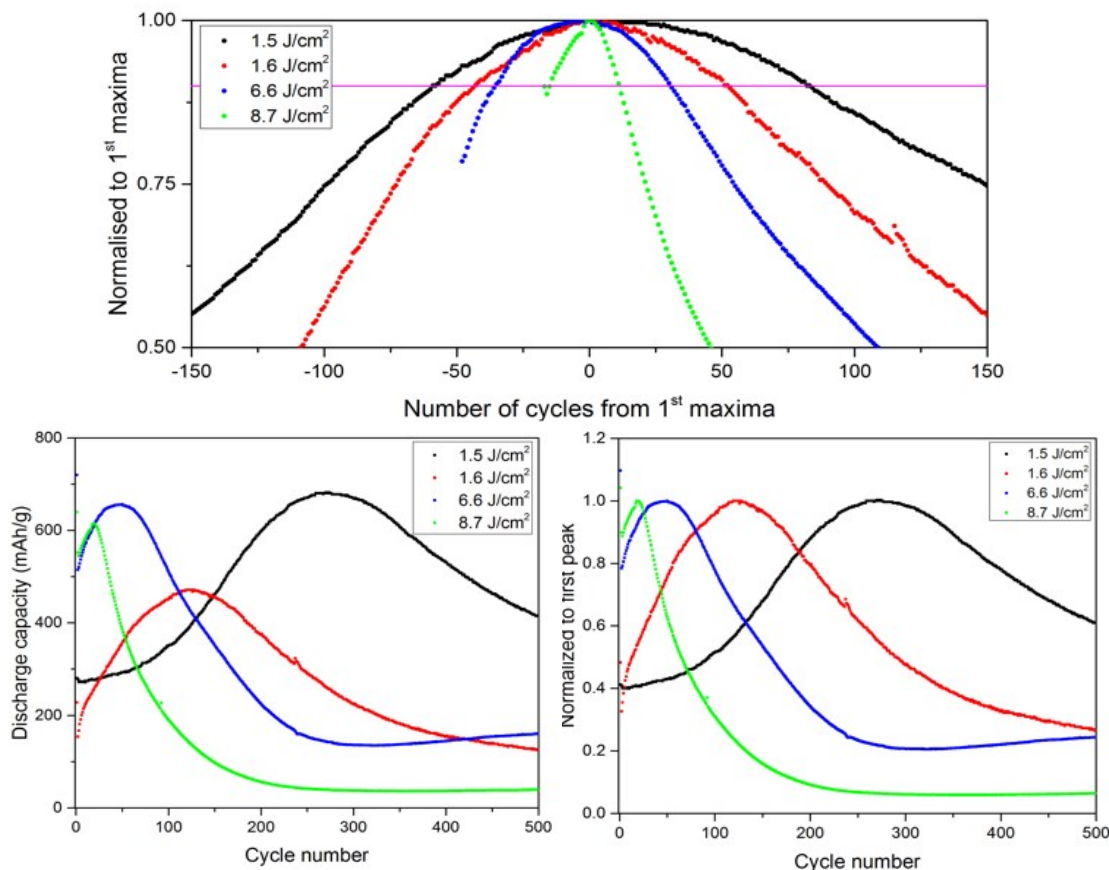


Figure S6(a). Cycles around 1<sup>st</sup> maxima or peak capacity for thick Cu films, demonstrating the broadness of the peaks compared to laser energy. (b) Raw discharge capacity versus cycle number and peak maxima normalised to the 1<sup>st</sup> capacity maxima.

### Electrochemical variation

Variation of electrochemistry was used as another test of the robustness of the electrodes. The cycling performance of a film grown on a thin Cu substrate at 1.5 J/cm<sup>2</sup> can be viewed in Figure S7. The film was cycled at a higher current rate of 15.8 A/g then the thin Cu cell discussed above and produced an initial capacity of 79 mAh/g. The higher current applied results in a lower capacity (without the 0.3 A/g initiation cycle). The electrode experiences an unusually gradual increase to the maximum not seen in other electrodes. The electrode exhibits a plateau around 109 mAh/g lasting from cycle 12016 to 16287 and then decreased to 63 mAh/g at cycle 42848. The electrode was then rested for four hours which initiated an increase to 123 mAh/g. This was followed by the peak capacity of 434 mAh/g at cycle 43081. On close inspection of this peak two distinct slopes can be seen. An initial slope with a gradient of  $4.96 \pm 0.06$  mAh/g/cycle which decreases to  $0.572 \pm 0.004$  mAh/g/cycle at cycle 42900 to the peak capacity. There is a decreasing slope of  $-1.97 \pm 0.008$  mAh/g/cycle for the decreasing capacity component of the peak. Interestingly it takes about 230 cycles for the capacity to both reach its peak capacity and return to its pre-maxima value. However, it takes about 18000 cycles for the capacity to reach its 2<sup>nd</sup> peak capacity of 587 mAh/g at cycle 76233. Interestingly it takes 25898 cycles to lose only 20% of this value. The electrode is currently still cycling and has a capacity of 469 mAh/g at cycle 102131. It should also be noted that the electrodes highest capacity of 600 mAh/g was reached at cycle 93202 and was caused by a phenomena present in multiple electrodes where we see relatively small local minima and maxima in capacity - this has yet to be investigated. A capacity of 600 mAh/g at 15.8 A/g is an astonishing achievement over 93202 cycles. The closest high rate literature example of MoO<sub>2</sub> demonstrates a capacity of 300 mAh/g at 10 A/g over 10000 cycles (1).

Figure S8a shows a cycling data comparison of two films deposited on a thick Cu substrate at 1.5 and 6.6 J/cm<sup>2</sup> with thicknesses of 103 and 392 nm. The films were cycled at 7.7 and 2.0 A/g respectively. The film cycled at 7.7 A/g had a smaller potential window of 0.2 – 3.0 V up until cycle 5747 where it was shifted to have the same potential window as the 2.0 A/g film of 0.02 – 3.0 V. As expected, the electrode cycled at 2.0 A/g had a higher initial capacity of 720 mAh/g, compared to 281 mAh/g for the electrode cycled at 7.7 A/g. Interestingly this was not the case for the (1<sup>st</sup>) peak capacity of each electrode as they had comparable capacities of 681 and 656 mAh/g for the 7.7 and 2.0 A/g electrodes respectively. It is also interesting that the electrode cycled at 2.0 A/g features an increasing capacity at the 3000<sup>th</sup> cycle. The results can be

explained by the combination of mass, thickness and available surface area of the electrodes. That is, the film deposited at  $6.6 \text{ J/cm}^2$  has a large percentage of its mass not participating in the storage of Li ions during the early stages of cycling. As cycling progresses the peak capacity mechanism possibly allows access to the lower layers of the film.

A film grown on thin Cu at  $1.6 \text{ J/cm}^2$  (Figure S8b) underwent an initial cycle at  $0.3 \text{ A/g}$  followed by cycling at  $1.5 \text{ A/g}$  where the capacity dropped from  $290$  to  $179 \text{ mAh/g}$ . Every  $1000^{\text{th}}$  cycle it performed one cycle at  $0.3 \text{ A/g}$ . The electrode was removed from the coin cell at cycle  $167$  for XRD analysis (Point A Figure S8b) where it showed only Cu peaks in the charged state. Upon returning the electrode to a coin cell the capacity dropped from  $482$  to  $280$  and then  $145 \text{ mAh/g}$  in subsequent cycles. The capacity then climbed steadily until cycle  $1002$  where the current rate was dropped to  $0.3 \text{ A/g}$  for a single cycle. This caused the capacity to jump from  $251$  to  $452 \text{ mAh/g}$  (Point B Figure S8b). Interestingly when returning to  $1.5 \text{ A/g}$  it held a capacity of  $452 \text{ mAh/g}$  for one cycle before dropping to  $407 \text{ mAh/g}$ . The capacity then increased to  $709 \text{ mAh/g}$  at cycle  $1194$  (Point C Figure S8b). Following this the battery was rested and the potential window was increased. The lower potential was shifted from  $0.2$  to  $0.02 \text{ V}$ . Upon re-initiating cycling at the larger potential window, the capacity dramatically increased to  $1131 \text{ mAh/g}$  and continued to increase until reaching a peak capacity of  $1342 \text{ mAh/g}$  at cycle  $1217$ . The capacity then began rapidly decreasing to a local minimum of  $188 \text{ mAh/g}$  at cycle  $1563$ . The electrode had a capacity of  $1714 \text{ mAh/g}$  at cycle  $3837$  and continued to increase. This value at the  $3837^{\text{th}}$  cycle makes this electrode the highest rated capacity in the literature of all  $\text{MoO}_x$  electrodes including  $\text{MoO}_x$ -carbon composites which have achieved capacities of  $1525$  and  $1600 \text{ mAh/g}$  (48,49). It is interesting to note that such high capacities are achieved even when the cell is disassembled and re-assembled and rested. Such high values of capacity illustrate the potential advantages of using PLD growth to generate thin-film based batteries. However, the cost of PLD and processing conditions needs to be taken into consideration when designing a device and therefore such high capacities with relatively expensive electrodes are likely to find specialist applications. Parallel implementation of the parameters could be transferred to sputtering techniques which are commonly used in industry.

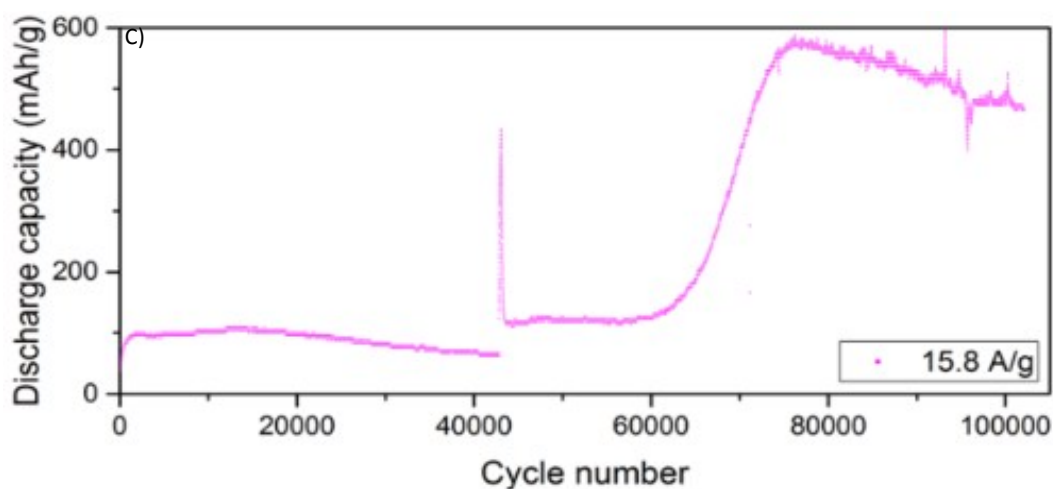
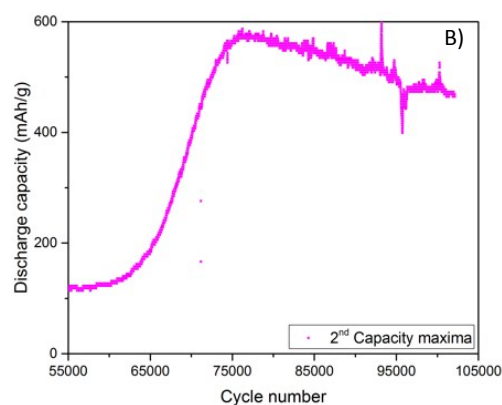
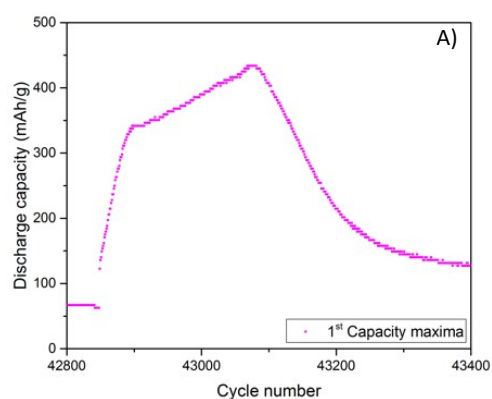


Figure S7. Magnified plots of (a) 1<sup>st</sup> peak capacity and (b) 2<sup>nd</sup> peak capacity. (c) Discharge capacity versus cycle number of electrode cycled at a current rate of 15.8 A/g.

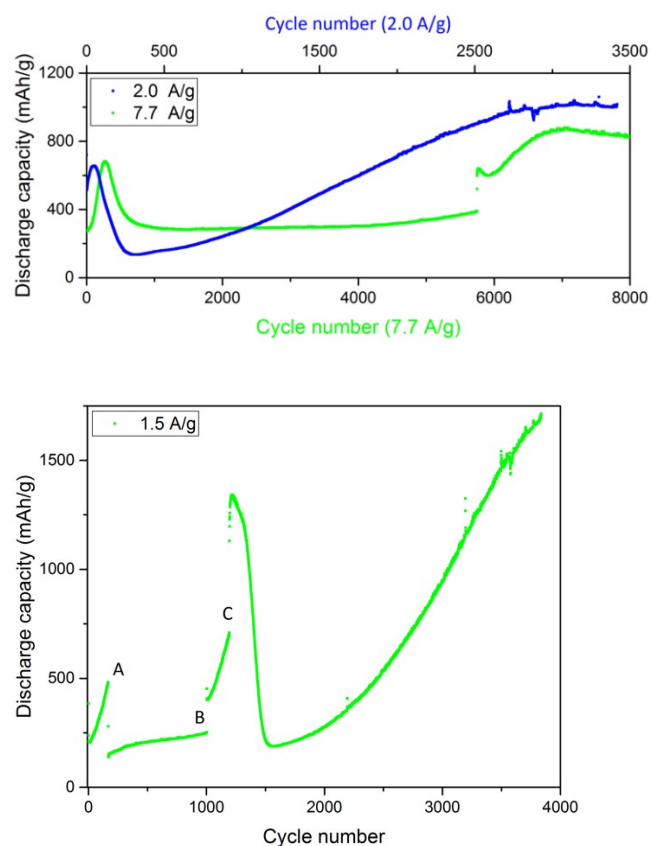


Figure S8. (a) Comparison of electrodes cycled at 2.5 and 7.7 A/g and (b) discharge capacity versus cycle number of an electrode cycled at 1.5 A/g

## References

- [1] Liu, M., Hou, X., Wang, T., Ma, Y., Sun, K., Liu, D., Wang, Y., He, D. and Li, J., 2018. Rapid activation and enhanced cycling stability of  $\text{Co}_3\text{O}_4$  microspheres decorated by N-doped amorphous carbon shell for advanced LIBs. *Electrochimica Acta*, 283, pp.979-986.